Non-linear enhancement of ultrafast X-ray diffraction through transient resonances

Tais Gorkhover (tais.gorkhover@cfel.de)
University of Hamburg
Stephan Kuschel
TU Darmstadt
Phay Ho
Argonne National Laboratory https://orcid.org/0000-0001-5214-2180
Andre Al Haddad
Paul Scherrer Institut
Felix Zimmermann
TU Berlin
Leonie Flückiger
La Trobe University
Matthew Ware
SLAC National Laboratory
Joseph Duris
SLAC National Laboratory
James MacArthur
SLAC National Laboratory
Alberto Lutman
SLAC National Accelerator Laboratory https://orcid.org/0000-0001-5791-9198
Ming-Fu Lin
SLAC National Accelerator Laboratory https://orcid.org/0000-0001-8086-2484
Xiang Li
SLAC National Accelerator Laboratory https://orcid.org/0000-0001-8338-4123
K. Nakarara
SLAC
Jeff Aldrich
SLAC National Accelerator Laboratory
Peter Walter
https://orcid.org/0000-0001-8839-1154
Linda Young
Argonne National Laboratory https://orcid.org/0000-0002-2251-039X
Christoph Bostedt

Paul Scherrer Institute
Agostino Marinelli
SLAC National Accelerator Laboratory https://orcid.org/0000-0002-7248-4652

Article

Keywords:

Posted Date: January 22nd, 2024

DOI: https://doi.org/10.21203/rs.3.rs-3776765/v1

Additional Declarations: There is **NO** Competing Interest.

Non-linear enhancement of ultrafast X-ray diffraction through transient resonances

Stephan Kuschel[1,2,3,11*], Phay J. Ho[4 *], Andre Al Haddad[4,5], Felix F. Zimmermann[2,3,6], Leonie Flueckiger[7], Matthew R. Ware[2,3], Joseph Duris[3], James P. MacArthur[3], Alberto Lutman[3], Ming-Fu Lin[3], Xiang Li[3,8], Kazutaka Nakahara[3], Jeff W. Aldrich[3], Peter Walter[3], Linda Young[4,9], Christoph Bostedt[4,5,10], Agostino Marinelli[3*], and Tais Gorkhover[1,2,3*]

[1]University of Hamburg, Institute for Experimental Physics/CFEL, Luruper Chaussee 149 22761 Hamburg, Germany
[2]Stanford PULSE Institute, SLAC National Accelerator Laboratory, 2575 Sand Hill Rd, Menlo Park, CA 94025, USA
[3]SLAC National Accelerator Laboratory, 2575 Sand Hill Rd, Menlo Park, CA 94025, USA
[4]Chemical Sciences and Engineering Division, Argonne National Laboratory, 9700 S. Cass Avenue, Lemont, IL 60439, USA
[5]Paul Scherrer Institute, 5232 Villigen, Switzerland
[6]IOAP, TU Berlin, Hardenbergstrasse 36, 10623 Berlin
[7]La Trobe University, 1300 La Trobe, Australia
[8]J.R. Macdonald Laboratory, Department of Physics, Kansas State University, Manhattan, Kansas 66506, USA
[9]Department of Physics and James Franck Institute, The University of Chicago, Chicago, IL 60637, USA
[10]LUXS Laboratory for Ultrafast X-ray Sciences, Institute of Chemical Sciences and Engineering, École Polytechnique Fédérale de Lausanne (EPFL), CH-1015 Lausanne, Switzerland
[11]Technical University Darmstadt, Institute of nuclear physics, Schlossgartenstr. 9, 64289 Darmstadt, Germany
*stephan.kuschel@tu-darmstadt.de
*tais.gorkhover@cfel.de
*pho@anl.gov
*marinelli@slac.stanford.edu

ABSTRACT

Diffraction-before-destruction imaging with ultrashort X-ray pulses can visualise non-equilibrium processes, such as chemical reactions, with sub-femtosecond precision in the native environment without the need of crystallization. Here, a nanospecimen diffracts a single X-ray flash before the sample disintegrates. The structure of the specimen is reconstructed from the coherent diffraction image (CDI). Such state-of-the-art X-ray snapshots lack high spatial resolution information due to weak diffraction signal i.e. shot noise. Bleaching effects from photo-ionization significantly restrain image brightness scaling and thus, further improvement of the spatial resolution. We find that non-linear transient form factor changes can overcome this barrier if FEL pulses are shorter than those applied in the majority of previous experiments. We compared snapshots from individual $\approx 100\,\mathrm{nm}$ Xe nanoparticles as a function of the X-ray pulse duration and incoming X-ray fluence in the vicinity of the Xe M-shell resonance. Surprisingly, images recorded with few to sub-femtosecond pulses are up to 10 times brighter than the semi-classical model predicts. Our Monte-Carlo simulation suggests that transient ion form factors can increase the brightness of X-ray images by several orders of magnitude. This provides a novel avenue towards significant improvement of the spatial resolution in CDI in combination with sub-fs temporal precision at the nanoscale.

The combination of coherent diffraction imaging (CDI) with bright and focused femtosecond short flashes from X-ray Free Electron lasers (FELs)[1–5] has brought to light transient non-equilibrium phenomena such as metastable stages of metal nanoparticle formation[6], unexpected morphologies diversity in soot formation[7], complex light matter interaction dynamics[3,4,8–12], vortex organisation in superfluid droplets[13], relaxation of superheated particles on the femtosecond time scale[8,11,14] and otherwise inaccessible states of water[15]. Theoretical studies suggest that sub-nm spatial resolution within a single FEL exposure is feasible under ideal FEL pulse conditions[1,16–19]. Such spatial resolution in combination with sub-fs temporal precision would transform our capabilities to follow ultrafast phase transitions, photo-chemical or catalytic reactions at the single nanoparticle level in native state. However,

state-of-the-art spatial resolution in experiments on individual heavy element nanoparticles is limited to a few nanometers even in the hard X-ray regime[19–22]. Further increase in spatial resolution requires an enhancement in diffraction image brightness. In the linear semiclassical model, the scattered photon number from a specimen is proportional to the incoming X-ray photon fluence F_{ph} (incoming photons per area) and a constant, wavelength specific elastic scattering cross section σ_{scat} of the material[23–25]. This assumption breaks down for high FEL fluences when the image brightness is affected by bleaching effects inside the sample, which reduce the effective scattering cross section during the FEL exposure[10,16,19,20,26–32].

Bleaching is a result of a complex interplay between electronic and ionic structural damage of the sample interacting with an intense X-ray FEL pulse. Electronic damage is initiated by photoionisation processes, which are inevitable when the specimen is exposed to intense X-ray pulses. Sequential multi-photon absorption and subsequent relaxation processes such as Auger/Coster-Kronig decays remove the electrons from the parent ions on sub-fs to 10-fs time scale. Ionisation increases the transparency of the sample as a shrinking number of bound electrons decreases the absorption/scattering cross sections of an ion according to the semi-classical model[26–28]. The subsequent damage to the ionic structure through hydrodynamic expansion is driven by the hot electrons trapped by a rapid build up of space charge[8,33]. There is a consensus that the FEL pulse duration must be shorter than the anticipated onset of ionic structure damage. But electronic structure modification cannot be avoided during the FEL exposure. Thus, most studies regard electronic bleaching through photoionisation as an inevitable limit to image brightness scaling with F_{ph}, which is detrimental to the quality of the diffraction images[17,19,20,20,28–30,32].

Non-linear scattering response in X-ray diffraction images of single nanoparticles

In contrast to previous studies, we find a more complex picture where increased F_{ph} leads to higher photoionisation rates but also to enhancement of the effective scattering cross section if FEL pulses are extremely short and tailored to excite multiple transient ion resonances. In our study, we explore the brightness and spatial resolution of diffraction images of individual Xe nanoparticles as a function of FEL pulse parameters such as FEL photon energy $h\nu$, pulse energy E_{p}, and duration τ (all parameters are summarized in Table 1, Supplements). We scanned the photon energy $h\nu$ in the vicinity of the Xe 3d absorption edge.

A detailed schematic of our experiment is exhibited in Figure 1, panel (a). Individual near-spherical Xe nanoparticles with diameters 60-150 nanometers intersect the path of focused and intense single X-ray FEL pulses inside the LAMP endstation at the Linac Coherent Light Source (LCLS)[34,35]. Single-particle, single-exposure X-ray diffraction snapshots are recorded at 30 Hz using p-n junction charge coupled devices (pnCCDs)[36] located at two different positions further downstream from the interaction region (see supplement, section Experimental setup). The particle size is directly encoded into the Airy pattern-like diffraction patterns and can be recovered with ± 0.3 nm precision (see supplement, section Cluster size fitting model). We scanned the photon energy $h\nu$ in the vicinity of the Xe 3d absorption edge between $650\,\mathrm{eV} < h\nu < 740\,\mathrm{eV}$. In addition, we recorded images at $h\nu = 1500\,\mathrm{eV}$ where transient resonances in Xe gas have been observed previously[37]. Each scanning step contains thousands of diffraction patterns from single Xe nanoparticles with fluctuating brightness due to random positions inside the 1.5 μm FEL focus with a near Gaussian X-ray fluence distribution[8]. We investigated three FEL pulse durations: 200 fs as a typical pulse duration preferred in most ultrafast CDI studies[5,7,19,38–40], 5-10 fs as a pulse duration beating the onset of the ionic structure damage of the specimen, and newly available sub-fs pulses[41] outrunning significant parts of electronic damage through relaxation processes such as Auger decay (Xe M-shell Auger life time $\approx$1 fs).

The comparison of the brightest images for each pulse duration sheds light on the scattering efficiency at different time scales. Some of the brightest single X-ray diffraction snapshots per FEL pulse duration are displayed on the left side of Figure 1 in (b)-(d). The diffraction patterns stem from similarly sized nanoparticles with diameters 97 ± 3 nm. Intuitively, one would expect that the brightest images are recorded using 200 fs pulse with the highest pulse energy $E_p = 1.5\,\mathrm{mJ}$ which corresponds to the highest fluence F_{ph} (panel (b)). In fact, the most intense X-ray diffraction snapshots were taken with few femtosecond pulses and only $E_p = 0.1\,\mathrm{mJ}$ (Figure 1, panel (d)).

The strong non-linearity of the measured scattering process emerges from a comparison between the experimental

data and the simulation of the anticipated images based on the linear semi-classical model[42]. Here we assume that the brightest images originate from the vicinity of the FEL focus center with F_{ph}^{max}. The right hand side images in Figure 1 (b)-(d) display extrapolated brightest shots based on linear scaling with F_{ph}^{max} and literature values of σ_{scat}. The values for F_{ph}^{max} are deduced from beam line parameters and statistical data analysis (see supplement, section Experimental Setup). The images recorded with sub-fs and few fs FEL pulses appear brighter than linear scaling with F_{ph}^{max} would predict. In contrast, the experimental diffraction patterns recorded with 200 fs and highest F_{ph}^{max} are one order of magnitude dimer.

This observation points to a complex interplay between electronic and ionic damage occurring on different time scales. The dim 200 fs images could be explained by typical bleaching and ion structural damage observed in previous studies. However, the brightness enhancement for 5 fs and sub-fs exposures hints at non-linear effects such as transient resonances (TRs) which can emerge during the FEL exposure.

Theoretical model of transient resonances

TRs arise when core-hole ionisation events drive the parent ion into short-lived resonances[3,4,9,30,43,44]. Previous studies in rare gas atoms reported increases in absorption cross section by almost two orders of magnitude due to individual transient resonances in Ne[43] and even transient resonances cascades in Xe atoms at 1500 eV[44]. The potential of transient resonances for imaging has received little attention so far as first imaging experiments with 100-200 fs long pulses on single nanoparticles suggested rather detrimental effects[3,4,9,30].

The TR mechanism is illustrated in Figure 2 based on the mechanism of 3d $\rightarrow$ 4f resonant X-ray scattering in a neutral Xe atom and a core-excited Xe+* ion. Resonant scattering occurs through virtual electron transitions between the 3d core level and the unoccupied 4f state as illustrated for neutral Xe (Figure 2 (a)). If X-rays are scattered by the core-hole excited Xe+* ion with a modified Coulomb potential (Figure 2 (b)), the binding energy of the excited 3d* orbital shifts from $h\nu_1$ (black dashed arrows) to $h\nu_2^* \approx h\nu_1 + 40$ eV (red arrows). In addition, the 4f* orbital in Xe+* is pulled closer towards the core in order to screen the positive charge, as visualised by the absolute value of the wave function $|\psi|$ (Figure 2 (b), top graph). This orbital restructuring increases the overlap between the 3d* and 4f* orbitals and thus, the transition dipole moments. The resulting augmented 3d* $\rightarrow$ 4f* scattering cross section σ_{scat}^* is more than one order of magnitude higher than the neutral Xe σ_{scat}(red vs black dotted line in Figure 2 (c), (see supplement, section Simulation).

The overall lifetime of a single transient resonance is limited by the core-hole decay time and by the photoionisation rate. However, multiple TRs pathways can appear as the FEL pulse excites a range of ionization states. A previous absorption spectroscopy study on FEL ionized Xe atoms suggested that sequential multi-photon absorption can trigger TR cascades throughout the entire FEL exposure duration at $h\nu \approx 1500$ eV[44]. Such TR cascades arise if more than one photon per atom is absorbed as demonstrated by our ion state matrix calculation. In Figure 2 (d), the colour scale indicates the changes in scattering cross section σ_{scat}^* of different excited Xe ions normalized by the neutral Xe σ_{scat}. During the FEL pulse exposure in the soft X-ray region, the most likely photo-ionization process is the removal of a single core M-shell electron (number of the core cores is on the Y axis). Depending on the FEL fluence and photon energy, subsequent core holes can be created through sequential photo-ionisation. Such highly excited ions usually recombine through Auger decay and open new vacancies in the valence shells within femtoseconds (number of valence holes is on the X-axis). Nanoplasma effects such as collisional and frustrated ionization can further promote the removal of outer shell electrons[3,4,8].

Above the M-shell absorption edge at $h\nu = 730$ eV , σ_{scat}^* of Xe ions with charge states 1+ to 20+ are at least one order of magnitude greater than σ_{scat} as demonstrated in Figure 2, upper panel (d). If more than one X-ray photon per Xe atom is absorbed on average, the Xe ions inside the nanoparticles will run through a series of excitation and relaxation channels which will contribute to the enhancement of the integrated σ_{scat}^* throughout the FEL exposure. The relaxation processes will reduce the number of core-holes but increase the valence vacant states which also exhibit enhanced σ_{scat}^*. Far above the Xe M-edge at 1500 eV brighter images can be expected if the FEL pulses can produce double core holes as exhibited in Figure 2, lower panel (d). The σ_{scat}^* of a double core Xe ion scatters over 10 time more efficiently than σ_{scat}. After few femtoseconds, such core holes can relax and produce a highly charged

nanoplasma with valence vacancies 20+ and higher[11,37] which will drive the system into a relaxation/excitation cascades with enhanced σ^*_{scat}.

Transient resonances benefit image quality if the FEL exposure is very short

Such TR cascades at photon energies above classical absorption edges provide a new dimension to counter and even overcompensate bleaching effects if the FEL parameters are chosen appropriately. One important aspect is that increased σ^*_{scat} comes often at the cost of enhanced absorption cross sections of ions as both cross sections are intertwined through Kramers-Kronig relations. Stronger absorption cross sections ultimately means that ionic structure damage is accelerated and thus, FEL pulse durations considered standard for imaging might result in degraded images if the FEL pulses are very intense. A statistical analysis of the scattering cross sections σ^{exp}_{scat} extracted from thousands of recorded images supports the hypothesis that resonant X-ray diffraction from excited ions can be both, detrimental or beneficial to the image brightness and quality. Our data overview illuminates the full extent of bleaching in 200-fs snapshots and the enhancement of σ_{exp} in diffraction patterns recorded with sub-fs and few-fs pulses as summarized in panels (a)-(c) in Figure 3. We calculated σ^{exp}_{scat} per Xe atom for the top 5 % brightest images for each incoming X-ray photon energy scan step. Each dot represents a single measured diffraction image of an individual Xe nanoparticle which is sufficiently bright for an automated nanoparticle size fitting routine (see supplement, section Cluster size fitting model). The individual value for σ^{exp}_{scat} for the top 5 % shots can be directly deduced from the image brightness corrected for the exposure fluence F_{ph} and the nanoparticle size (see supplement, section Calculation of the scattering cross section). The absolute value for F_{ph} has been cross checked using a calibration correlating the measured M-shell fluorescence yield (see supplement, section Signature of transient resonances in the fluorescence yield), and the pulse energy values reported by the gas detector (see supplement, section Experimental setup).

The corresponding literature values for σ_{scat} for the neutral Xe atom are visualised by the dashed gray line[45]. For all pulse durations, σ^{exp}_{scat} values follow closely the literature Xe values near the M shell 3d resonance ($h\nu < 720\,\mathrm{eV}$) with the exception of most intense 200 fs pulses. The situation changes above the M-edge. First, for all three pulse durations, conditions above the M-shell exist when σ_{exp} significantly exceed the Xe literature value for the corresponding photon energy above 720 eV (see arrows in Figure 3, panels (a)-(c)) . In all σ_{exp} enhancement cases, coincident measurements of fluorescence yield confirm that on average more than one X-ray photon per atom has been absorbed (see supplement, section Signature of transient resonances in the fluorescence yield). For short pulses, brightness of the images can increase non-linearly with incoming fluence. At $h\nu = 1500\,\mathrm{eV}$ and 5-10 fs pulse duration (red dots), the enhancement is $\sim$10 times higher than any point on the dotted Xe literature value curve and also in comparison with weaker FEL pulses (blue dots). Second, for longer pulses the role of TRs is more ambiguous. The σ_{exp} extracted from images recorded with 200-fs and $E_p = 1.5$ mJ pulses (blue dots) is overall 10 times lower than Xe literature values. When 200 fs pulses are attenuated, σ_{exp} is augmented for photon energies above the M-shell.

Our simulated σ^*_{scat}[32] (solid lines in (a)-(c) in Figure 3) is overall in good agreement with corresponding σ_{exp}. For 200 fs FEL exposures with $E_p = 1.5$ mJ pulses, our calculation predicts a significant lowering of the scattering cross section because of the rapid disintegration of the ion structure fuelled by transient resonances (see supplement, section Simulation Results, Figure 4). The presence of transient resonances above the 3d M-shell absorption edge for shorter and/or longer but weaker pulses is also supported by our calculation. If the sample is exposed to attenuated 200 fs pulses, the hydrodynamic expansion occurs much slower and thus, the scattering enhancement of TRs reappear. Interestingly, the simulation underestimates the non-linear scattering enhancement at $h\nu = 1500\,\mathrm{eV}$. One possible reason is that our simulation neglects ionisation potential suppression[46,47] which can rapidly delocalise the valence electron shells and lead to extremely efficient transient resonance cascades[33]. Assuming that Xe $n = 5$ and $n = 4$ shells are fully removed, our simulation predicts σ^*_{scat} up to 9 times the neutral Xe cross section for 5-10 fs FEL pulses at $h\nu = 1500\,eV$ in agreement with our data. An indirect support for a significant role of complex nanoplasma ionization effects stems from coincident extreme fluorescence yield (see supplement, section Signature of transient resonances in the fluorescence yield).

The increase in scattering cross section for short pulses directly translates into higher resolution as pointed out in Figure 3, panel (d). The radial plot of one of the brightest diffraction patterns from a single Xe cluster (red line) maintains a high signal to noise ratio down to 5-6 nm full period resolution (see supplement, section Single exposure images)). This is comparable to the best spatial resolution achieved so far in single shot X-ray imaging with higher-Z Au nanoparticles using hard X-rays with one order of magnitude shorter wavelengths[20].

Summary and Outlook

Overall, our study illuminates the potential of transient resonances in ultrafast X-ray CDI. We demonstrate that transient resonances can significantly increase the brightness of X-ray diffraction images if FEL pulses are shorter than the onset of the ionic structure damage. We observed the enhancement effect across at least one order of magnitude in FEL fluence for pulse durations < 10 fs. This data and our simulations indicate that the effect is scalable with FEL pulse energy as subsequent photoionisation events can drive the ions into a resonant cascade similar to REXMI[37] and some resonances enhance diffraction by factors up to $> 10^4$ (see Figure 2, panel (c) and (d)). TRs are not exclusive to Xe, previous spectroscopic studies have found short-lived resonances in oxygen[30] and neon[43]. In principle, TRs should also exist in the hard X-ray regime which offers a direct route to sub-nm resolution in single shot X-ray imaging. Beyond that, TRs are element specific and thus could increase material contrast in X-ray chemical femtosecond crystallography[48] and potentially eliminate the need of heavy stain atoms in time-resolved multi-wavelength anomalous crystallography studies. In principle, transient resonances can be excited by an optical pre-pulse and significantly increase signal-to-noise ratio in state-of-the-art ultrafast table-top XUV imaging setups[49].

Our study emphasizes the significance of intense and < 10 fs FEL pulses, which have received little attention so far in CDI. During the time of the present study, the FEL pulse energies for very short pulses were moderate and could not be easily scaled. Current developments in accelerator science are already changing the availability of very intense few fs and sub-fs pulses[41,50–52] . Newly available intense sub-fs FEL pulses can become a significant driver for ultrafast CDI as relaxation processes such as Auger decays of K- and L-shells happen mostly within hundreds of attoseconds. Our results pave the way for improvement of ultrafast CDI based on non-linear effects, which has the potential to combine atomic resolution with attosecond temporal precision. This will open new avenues for studies of non-equilibrium states of matter in chemistry and material science.

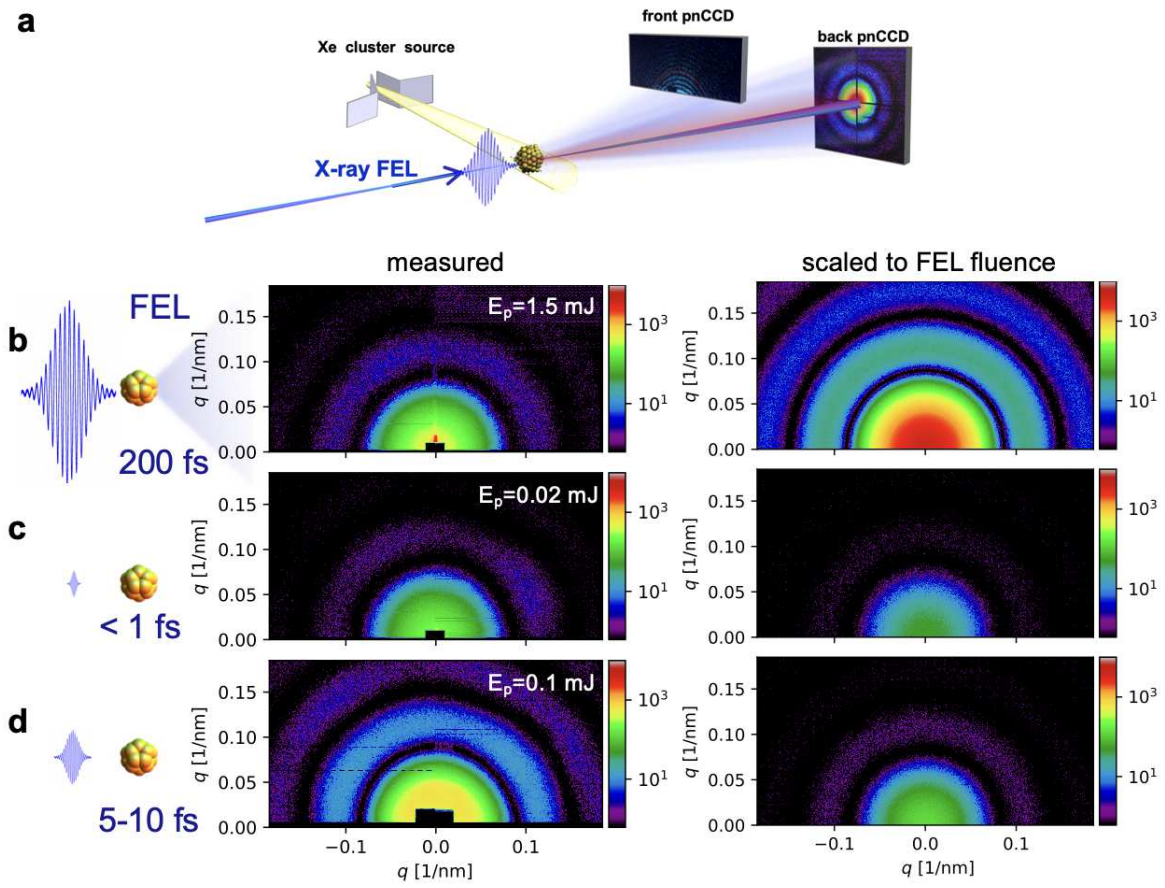

Figure 1. (a) The schematic of the experimental setup at the AMO Hutch at LCLS: Intense X-ray FEL pulses were focused and intersected with a stream of Xe clusters. The resulting single-shot, single-particle X-ray diffraction patterns were recorded using pnCCD detectors[34,36] positioned further downstream of the interaction point. The front pnCCD is positioned in a distance of 130 mm and the rear pnCCD at 732 mm from the X-ray focus. The brightest X-ray diffraction patterns of individual Xe nanoparticles with diameters 97±3 nm are displayed for (b) 200 fs, (c) 5-10 fs and (d) sub-fs pulse durations on the left side. The x and y axis of images recorded by the rear pnCCD are in plotted in q wave vector space. The colour scale indicates detected photons per pixel. The sub-fs image was recorded with a $E_p = 0.02$ mJ pulse energy at $h\nu = 735$ eV X-ray photon energy, the 200 fs with $E_p = 1.5$ mJ at $h\nu = 730$ eV, the 5 fs with $E_p = 0.1$ mJ pulse energy at $h\nu = 1500$ eV. The brightest image was not recorded using the strongest FEL pulse. The diffraction images expected from the semiclassical picture are plotted on the right side of (b)-(d). The right side images are calculated by Condor software[42] using the experimental FEL fluence listed in Table 1 and the quantum efficiencies of the pnCCD detector. According to linear scaling with incoming X-ray pulse energy one expects that the brightest X-ray diffraction snapshots should be observed from 1.5 mJ, 200 fs FEL pulses ((b),dark blue). In contrast, we find that the diffraction patterns which were recorded with only 0.1 mJ and 5 fs short pulses are the brightest. We attribute the increased brightness to transient resonances.

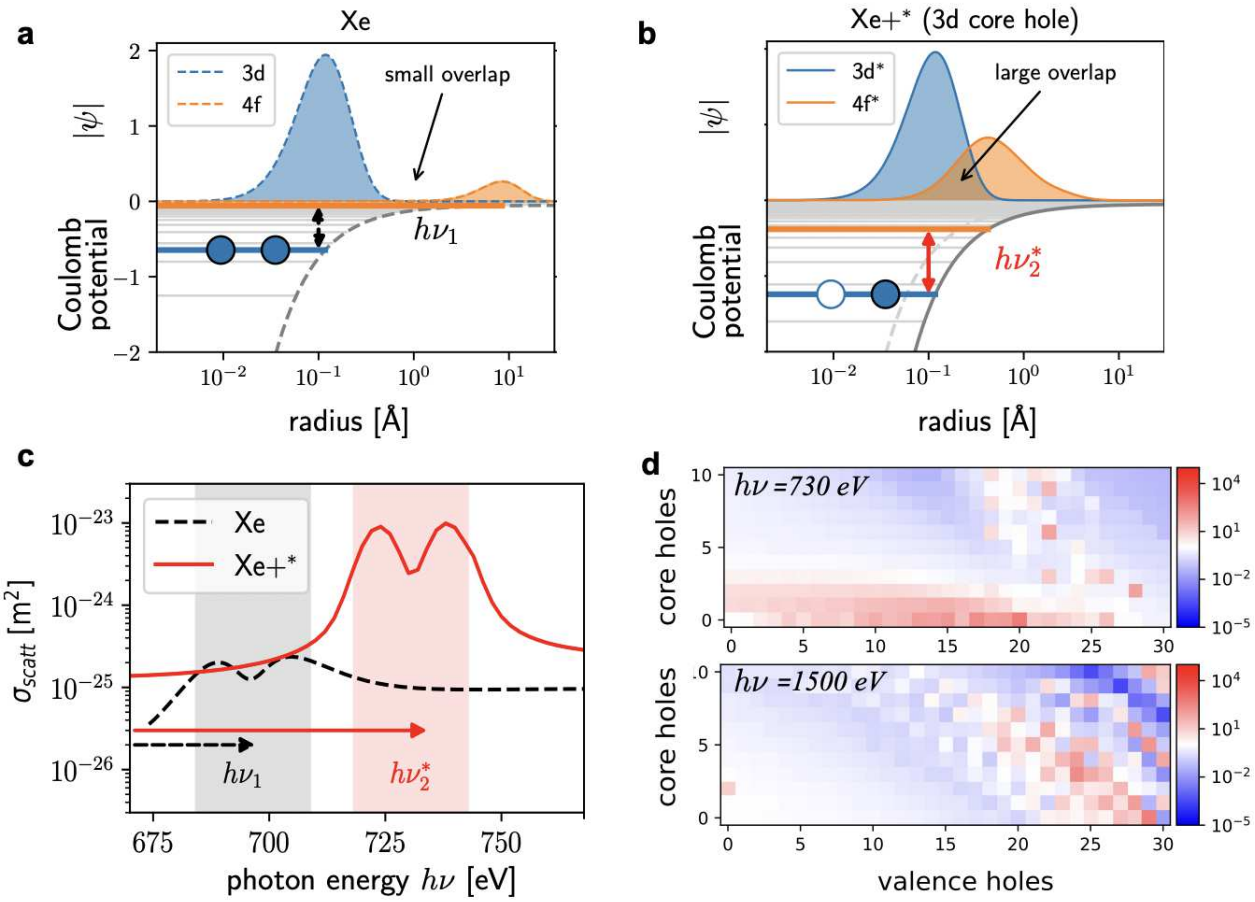

Figure 2. The concept of transient resonances: In (a), the Coulomb potential is plotted versus the distance from the charged core for a neutral Xe atom (gray dotted line) and in (b) for a core excited Xe+* (gray solid line). The corresponding 3d (blue) and 4f orbitals (orange) are displayed for a neutral Xe atom ((a), dashed lines) and 3d* and 4f* excited Xe ion with a core-hole ((b), solid lines). First, the core-hole excitation shifts the binding energy of the remaining 3d* electrons from $h\nu_1$ (black) to greater $h\nu_2^*$ (red) due to a modified Coulomb potential. Second, the core-hole excitation also rearranges the orbitals to 3d* (blue) and 4f* (orange) plotted on the top of the Coulomb potential. Due to the core-hole induced charge imbalance the 4f* orbital is pulled closer to the atom's center by almost two orders of magnitude creating a strongly increased overlap with the 3d* wave function and hence an increased transition dipole strength for the 3d* $\rightarrow$ 4f* transition. This has dramatic consequences for the scattering cross section in the vicinity of the Xe 3d absorption edge. In (c), the scattering cross section σ_{scat} for the neutral Xe (dashed black line) and σ_{scat}^* for the excited Xe+* (red solid line) is plotted vs the incoming X-ray photon energy. The excited atom Xe+* scatters two orders more strongly than neutral Xe at the shifted resonance position $h\nu_2^*$ and almost two orders more compared to the neutral Xe resonance maximum $h\nu_1$. Energies, cross-sections and radial wave functions displayed here were calculated using Hartree-Fock-Slater simulations (see supplement, section Simulations). Resonance maps for specific electronic states of Xe ions are depicted in (d). For a number of removed valence electrons (x-axis) and a number of removed inner shell 3d M-shell electrons (y-axis), the color scale displays the scattering cross section normalized by the neutral Xe cross section. At a photon energy $h\nu = 735$ eV (top graph) enhancement already sets in for low charge states, while at 1500 eV (lower graph) higher charge states are required for enhancement. The simulations suggest that a single charge state can scatter up to a factor 10^4 more than the neutral Xenon at 1500 eV.

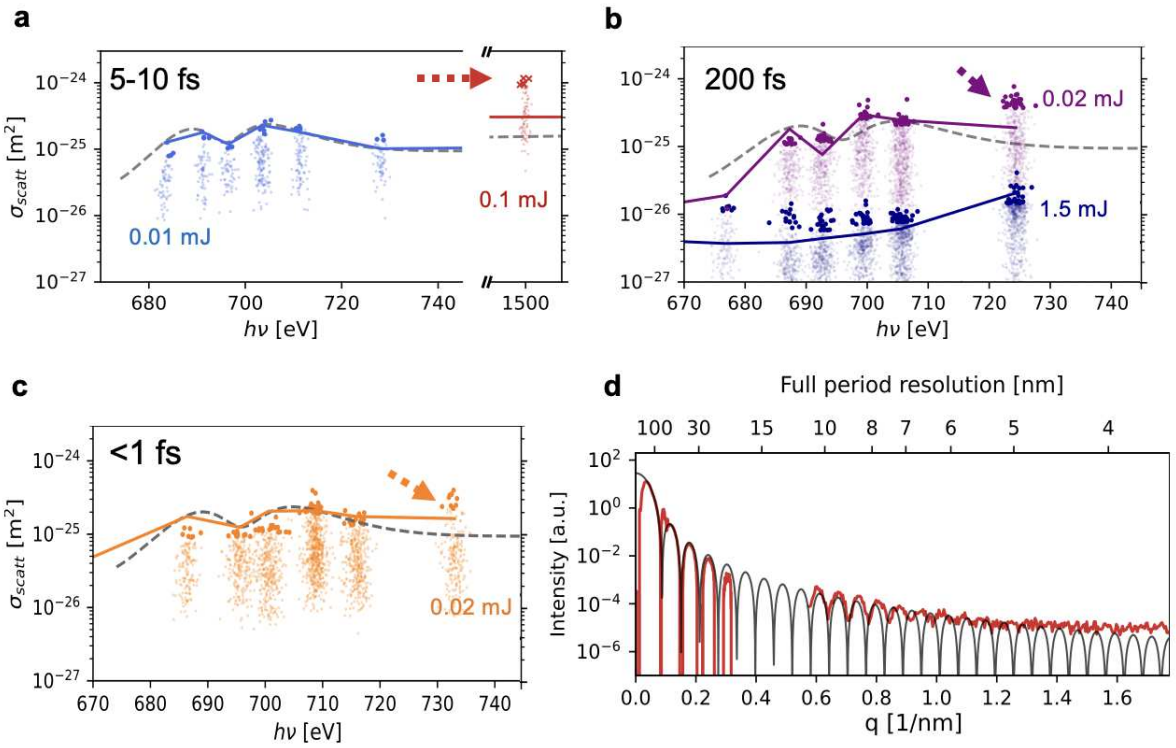

Figure 3. Panels (a)-(c) depicts the measured σ_{scat}^{exp} in dependence to the incoming X-ray photon energy $h\nu$ for all pulse duration measurements such as 5-10 fs (a), 200 fs (b) and 0.5 fs (c). Each dot in the graph represents a single Xe nanoparticle observed by a single FEL exposure. The point spread stems from the fact that the nanoparticle diameters 60-150 nm are much smaller than the FEL focus average full width half maximum (FWHM) 1.5 μm. Each randomly injected sample experiences a different exposure FEL fluence inside the FEL focus and only the top few percent of all hits with the highest fluorescence/scattering yields must have been recorded near the FEL focus center with the highest intensities. Thus, σ_{scat}^{exp} has been calculated only for the top 5% of all shots as indicated by bold dots (see supplement, section Calculation of the scattering cross section) and (see supplement, section Siganture of transient resonances in the fluorescence yield). The gray dashed line indicates the neutral Xe scattering cross section σ for comparison. Our calculations (solid lines) agree overall well with the experiment. The strongest enhancement can be found at 1500 eV (red) where TR cascades have been observed in the past in Xe atoms[37]. Above the M-edge, sub-fs pulses are scattered up to 4 times stronger than the linear model predicts. For further discussion see text. Panel (d) demonstrates that increased brightness translates to higher spatialresolution. Here, the radial plot (in red) of one of the brightest diffraction images recorded at 1500 eV is compared to theoretical diffraction signal from a solid sphere (black line). Diffraction signals down to 5-6 nm full period resolution are clearly visible and the overall radial profile follows closely the theoretical calculation for diffraction from a solid sphere.[4,9,28]. See Supplements, section Single e xposure images for the corresponding full detector images.

Acknowledgements

Use of the Linac Coherent Light Source (LCLS), SLAC National Accelerator Laboratory, is supported by the U.S. Department of Energy (DOE), Office of Science, Office of Basic Energy Sciences (BES) under Contract No. DE-AC02-76SF00515. S.K. and T.G. were supported by the U.S. DOE BES Chemical Sciences, Geosciences and Biosciences Division through the Panofsky fellowship from SLAC National Laboratory. PJH and LY were supported by the U.S. DOE BES Chemical Sciences, Geosciences and Biosciences Division under Contract No. DE-AC02- 06CH11357. F.Z.and M.R.W were supported by the U.S. DOE BES Chemical Sciences, Geosciences and Biosciences Division, Chemical Sciences, Geosciences and Biosciences Division through the Early-Career Research Program project number 100482.

Author contributions statement

T.G. and A.M conceived the idea for the experiment based on discussions with C.B., J.D., J.P.MA., A.L., and A.M. developed and operated the XLEAP sub-fs mode. M.-F.L., X.L., K.N., J.W.A., and P.W. prepared the beam line for the experiment. The experimental setup was planned and performed by all authors. S.K. led the data analysis. P.J.H performed the simulation of the experimental observations. S.K, P.J.H., C.B. and T.G. wrote the manuscript with input from all authors. All authors reviewed the manuscript.

Additional information

The authors declare no competing interests.

References

1. Neutze, R., Wouts, R., van der Spoel, D. & Weckert, J., E.and Hajdu. Potential for biomolecular imaging with femtosecond x-ray pulses. *Nature* **406**, 752 (2000).
2. Chapman, H. N. *et al.* Femtosecond time-delay x-ray holography. *Nature* **448**, 676–679 (2007).
3. Bostedt, C. *et al.* Clusters in intense flash pulses: ultrafast ionization dynamics and electron emission studied with spectroscopic and scattering techniques. *J. Phys. B* **12**, 083004 (2010).
4. Bostedt, C. *et al.* Ultrafast X-Ray Scattering of Xenon Nanoparticles: Imaging Transient States of Matter. *Phys. Rev. Lett.* **108**, 093401, DOI: 10.1103/PhysRevLett.108.093401 (2012).
5. Gorkhover, T. *et al.* Femtosecond X-ray Fourier holography imaging of free-flying nanoparticles. *Nat. Photonics* **12**, 150–153, DOI: 10.1038/s41566-018-0110-y (2018). 1707.09424.
6. Barke, I. *et al.* The 3D-architecture of individual free silver nanoparticles captured by X-ray scattering. *Nat. Commun.* **6**, 6187, DOI: 10.1038/ncomms7187 (2015).
7. Loh, N. D. *et al.* Fractal morphology, imaging and mass spectrometry of single aerosol particles in flight. *Nature* **486**, 513–517 (2012).
8. Gorkhover, T. *et al.* Nanoplasma dynamics of single large xenon clusters irradiated with superintense X-ray pulses from the linac coherent light source free-electron laser. *Phys. Rev. Lett.* **108**, 1–5, DOI: 10.1103/PhysRevLett.108.245005 (2012).
9. Rupp, D. *et al.* Imaging plasma formation in isolated nanoparticles with ultrafast resonant scattering. *Struct. Dyn.* **7**, DOI: 10.1063/4.0000006 (2020).
10. Ferguson, K. R. *et al.* Transient lattice contraction in the solid-to-plasma transition. *Sci. Adv.* **2**, e1500837–e1500837, DOI: 10.1126/sciadv.1500837 (2016).
11. Gorkhover, T. *et al.* Femtosecond and nanometre visualization of structural dynamics in superheated nanoparticles. *Nat. Photonics* **10**, 93–97, DOI: 10.1038/nphoton.2015.264 (2016). NIHMS150003.

12. Ihm, Y. *et al.* Direct observation of picosecond melting and disintegration of metallic nanoparticles. *Nat. communications* **10**, 1–6 (2019).

13. Gomez, L. F. *et al.* Shapes and vorticities of superfluid helium nanodroplets. *Science* **345**, 906–909 (2014).

14. Peltz, C. *et al.* Few-femtosecond resolved imaging of laser-driven nanoplasma expansion. *New J. Phys.* (2022).

15. Amann-Winkel, K. *et al.* Liquid-liquid phase separation in supercooled water from ultrafast heating of low-density amorphous ice. *Nat. Commun.* **14**, 442 (2023).

16. Ho, P. J. *et al.* Atomistic three-dimensional coherent x-ray imaging of nonbiological systems. *Phys. Rev. A* **94**, 063823, DOI: 10.1103/PhysRevA.94.063823 (2016).

17. Son, S.-K., Young, L., Santra, R. *et al.* Impact of hollow-atom formation on coherent x-ray scattering at high intensity. *Phys. Rev. A* **83**, 033402 (2011).

18. Schropp, A. & Schroer, C. G. Dose requirements for resolving a given feature in an object by coherent x-ray diffraction imaging. *New J. Phys.* **12**, DOI: 10.1088/1367-2630/12/3/035016 (2010).

19. Aquila, A. *et al.* The LINAC coherent light source single particle imaging road map. *Struct. Dyn.* **2**, 041701 (2015).

20. Ayyer, K. *et al.* 3d diffractive imaging of nanoparticle ensembles using an x-ray laser. *Optica* **8**, 15–23, DOI: 10.1364/OPTICA.410851 (2021).

21. Xu, R. *et al.* Single-shot three-dimensional structure determination of nanocrystals with femtosecond x-ray free-electron laser pulses. *Nat. communications* **5**, 1–9 (2014).

22. Yumoto, H. *et al.* High-fluence and high-gain multilayer focusing optics to enhance spatial resolution in femtosecond x-ray laser imaging. *Nat. communications* **13**, 1–8 (2022).

23. Guinier, A. & Fournet, G. *Small-angle scattering of X-rays*. Structure of matter series (Wiley, 1955).

24. Attwood, D. *Soft X-Rays and Extreme Ultraviolet Radiation* (Cambridge University Press, 2012).

25. Howellst, M. & Jacobsen, C. Soft X-ray Microscopes and their Biological Applications. *Q. Rev. Biophys.* **28**, 33–130, DOI: 10.1017/S0033583500003139 (1995).

26. Young, L. *et al.* Femtosecond electronic response of atoms to ultra-intense X-rays. *Nature* **466**, 56–61, DOI: 10.1038/nature09177 (2010).

27. Son, S. K., Young, L. & Santra, R. Impact of hollow-atom formation on coherent x-ray scattering at high intensity. *Phys. Rev. A - At. Mol. Opt. Phys.* **83**, 1–11, DOI: 10.1103/PhysRevA.83.033402 (2011).

28. Hau-Riege, S. P. & Chapman, H. N. Modeling of the damage dynamics of nanospheres exposed to x-ray free-electron-laser radiation. *Phys. Rev. E* **77**, 041902 (2008).

29. Barty, A. *et al.* Self-terminating diffraction gates femtosecond x-ray nanocrystallography measurements. *Nat. Photonics* **6**, 35 (2011).

30. Ho, P. J. *et al.* The role of transient resonances for ultra-fast imaging of single sucrose nanoclusters. *Nat. communications* **11**, 1–9 (2020).

31. Schorb, S. *et al.* Size-dependent ultrafast ionization dynamics of nanoscale samples in intense femtosecond x-ray free-electron-laser pulses. *Phys. Rev. Lett.* **108**, 1–5, DOI: 10.1103/PhysRevLett.108.233401 (2012).

32. Ho, P. J. & Knight, C. Large-scale atomistic calculations of clusters in intense x-ray pulses. *J. Phys. B: At. Mol. Opt. Phys.* **50**, 104003 (2017).

33. Wabnitz, H. *et al.* Multiple ionization of atom clusters by intense soft x-rays from a free-electron laser. *Nature* **420**, 482 (2002).

34. Ferguson, K. R. *et al.* The atomic, molecular and optical science instrument at the linac coherent light source. *J. Synchrotron Radiat.* **22**, 492–497 (2015).

35. Emma, P. *et al.* First lasing and operation of an ångstrom-wavelength free-electron laser. *nature photonics* **4**, 641–647 (2010).

36. Strüder, L. *et al.* Large-format, high-speed, x-ray pnccds combined with electron and ion imaging spectrometers in a multipurpose chamber for experiments at 4th generation light sources. *Nucl. Instrum. Meth. A* **614**, 483 (2010).

37. Rudek, B. *et al.* Ultra-efficient ionization of heavy atoms by intense X-ray free-electron laser pulses. *Nat. Photonics* **6**, 858–865, DOI: 10.1038/nphoton.2012.261 (2012).

38. Hantke, M. F. *et al.* High-throughput imaging of heterogeneous cell organelles with an X-ray laser. *Nat. Photonics* **8**, 943–949, DOI: 10.1038/nphoton.2014.270 (2014).

39. Seibert, M. M. *et al.* Single mimivirus particles intercepted and imaged with an X-ray laser. *Nature* **470**, 78–81, DOI: 10.1038/nature09748 (2011).

40. Daurer, B. J. *et al.* Corrigendum: Experimental strategies for imaging bioparticles with femtosecond hard X-ray pulses (IUCrJ (2017) 4 (251-262) DOI: 10.1107/S2052252517003591). *IUCrJ* **6**, 500, DOI: 10.1107/S2052252519004317 (2019).

41. Duris, J. *et al.* Tunable isolated attosecond X-ray pulses with gigawatt peak power from a free-electron laser. *Nat. Photonics* **14**, 30–36, DOI: 10.1038/s41566-019-0549-5 (2020). 1906.10649.

42. Hantke, M. F., Ekeberg, T. & Maia, F. R. Condor: a simulation tool for flash x-ray imaging. *J. applied crystallography* **49**, 1356–1362 (2016).

43. Kanter, E. P. *et al.* Unveiling and driving hidden resonances with high-fluence, high-intensity X-ray pulses. *Phys. Rev. Lett.* **107**, 1–5, DOI: 10.1103/PhysRevLett.107.233001 (2011).

44. Rudek, B. *et al.* Ultra-efficient ionization of heavy atoms by intense X-ray free-electron laser pulses. *Nat. Photonics* **6**, 858–865, DOI: 10.1038/nphoton.2012.261 (2012).

45. Hubbell, J. H. *et al.* A Review, Bibliography, and Tabulation of K , L , and Higher Atomic Shell X-Ray Fluorescence Yields. *J. Phys. Chem. Ref. Data* **23**, 339–364, DOI: 10.1063/1.555955 (1994).

46. Stewart, J. C. & Pyatt Jr, K. D. Lowering of ionization potentials in plasmas. *The Astrophys. J.* **144**, 1203 (1966).

47. Son, S.-K. *et al.* Quantum-mechanical calculation of ionization-potential lowering in dense plasmas. *Phys. Rev. X* **4**, 031004 (2014).

48. Schriber, E. A. *et al.* Chemical crystallography by serial femtosecond x-ray diffraction. *Nature* **601**, 360–365 (2022).

49. Rupp, D. *et al.* Coherent diffractive imaging of single helium nanodroplets with a high harmonic generation source. *Nat. communications* **8**, 1–7 (2017).

50. Marinelli, A. *et al.* Optical Shaping of X-Ray Free-Electron Lasers. *Phys. Rev. Lett.* **116**, 1–5, DOI: 10.1103/PhysRevLett.116.254801 (2016).

51. Lutman, A. A. *et al.* Polarization control in an X-ray free-electron laser. *Nat. Photonics* **10**, 468–472, DOI: 10.1038/nphoton.2016.79 (2016).

52. Guetg, M. W. *et al.* Generation of high-power high-intensity short x-ray free-electron-laser pulses. *Phys. Rev. Lett.* **120**, 014801 (2018).

53. Herman, F. & Skillman, S. *Atomic structure calculations* (Englewood Cliffs, NJ:Prentice-Hall, Englewood Cliffs, New Jersey, 1963).

54. Ho, P. J., Bostedt, C., Schorb, S. & Young, L. Theoretical tracking of resonance-enhanced multiple ionization pathways in x-ray free-electron laser pulses. *Phys. Rev. Lett.* **113**, 253001, DOI: 10.1103/PhysRevLett.113.253001 (2014).

55. Emma, P. Attosecond x-ray pulses in the lcls using the slotted foil method. *SLAC pub* DOI: 10.2172/833050 (2004).

56. Klein, M. L. & Venables, J. A. Rare gas solids. *Acad. Press. Lond.* **2** (1977).

57. Flückiger, L. *et al.* Time-resolved x-ray imaging of a laser-induced nanoplasma and its neutral residuals. *New J. Phys.* **18**, 043017 (2016).

58. Deslattes, R. D. Photoionization of the *M* Shell of Xenon. *Phys. Rev. Lett.* **20**, 483–485, DOI: 10.1103/PhysRevLett.20.483 (1968).

Supplementary Files

This is a list of supplementary files associated with this preprint. Click to download.

- TransientResonancesSoftXrayTGSupplements.pdf